NANO LETTERS

pubs.acs.org/NanoLett

Letter

Simultaneous Selective Area Growth of Wurtzite and Zincblende Self-Catalyzed GaAs Nanowires on Silicon

Vladimir G. Dubrovskii,* Wonjong Kim, Valerio Piazza, Lucas Güniat, and Anna Fontcuberta i Morral

Cite This: *Nano Lett.* 2021, 21, 3139−3145

Read Online

ACCESS | Metrics & More | Article Recommendations | Supporting Information

ABSTRACT: Selective area epitaxy constitutes a mainstream method to obtain reproducible nanomaterials. As a counterpart, self-assembly allows their growth without costly substrate preparation, with the drawback of uncontrolled positioning. We propose a mixed approach in which self-assembly is limited to reduced regions on a patterned silicon substrate. While nanowires grow with a wide distribution of diameters, we note a mostly binary occurrence of crystal phases. Self-catalyzed GaAs nanowires form in either a wurtzite or zincblende phase in the same growth run. Quite surprisingly, thicker nanowires are wurtzite and thinner nanowires are zincblende, while the common view predicts the reverse trend. We relate this phenomenon to the influx of Ga adatoms by surface diffusion, which results in different contact angles of Ga droplets. We demonstrate the wurtzite phase of thick GaAs NWs up to 200 nm in diameter in the Au-free approach, which has not been achieved so far to our knowledge.

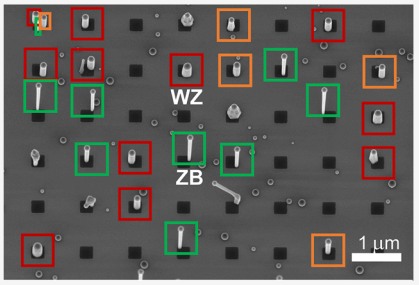

KEYWORDS: *GaAs nanowires, pinholes, crystal phase, contact angle, growth rate*

State of the art materials science and engineering correlate the growth conditions to a particular set of morphology, crystal phase, and functional properties. This is especially valid in epitaxy techniques, where the growth conditions are highly reproducible. Epitaxy at the nanoscale in the form of nanowires (NWs) or quantum structures has introduced more variability into the structural and functional outcome. This originates from statistical variations and size-dependent growth properties, which are amplified in the case of self-assembly.[1−3] Localized growth in predefined areas of a substrate constitutes one of the solutions to minimize these statistical variations. The growth sites can be defined by a regular array of metal particles catalyzing NW growth or by a patterned growth mask, resulting in selective area epitaxy.[4−6] A predefined distance between nanostructures guarantees the most similar growth conditions, given by the growth fluxes and modified by surface diffusion of species on the substrate.[7,8] Selective area epitaxy of NWs can result in freestanding or horizontally oriented structures, each configuration being suitable for different applications.[5,9−11] Freestanding vertical NWs are ideal for solar cell, light-emitting and photodetecting devices, while horizontal structures have opened new avenues for electronic devices, including quantum computing schemes.[12−14]

In this work, we present a variation of the principle of selective area epitaxy, which aims to join together the advantages of self-assembly and localized growth. We grow GaAs NWs by molecular beam epitaxy (MBE) in localized areas, surrounded by a 15 nm thick thermal SiO_2 acting as a mask on a silicon (111) substrate. The growth areas are arranged in a square lattice of 1 or 2 μm period (indicated as p in Figure 1). The size of the growth area (labeled as a in Figure 1) varies from 100 to 1000 nm. In each growth area, we allow a native oxide to form, as usually realized in self-assembly on silicon.[15] The periodic arrangement of the growth areas allows control of the precursors contributing to growth by direct impingement and surface diffusion. This can be achieved without the need for a high-precision patterning process. The scheme of this method, which we refer to as "localized self-assembled growth", is further elucidated in Figure 1.

GaAs NWs were grown on silicon substrates using the following protocol. The substrates were first degassed in an ultrahigh-vacuum (UHV) environment of an MBE machine (DCA P600) by annealing at 500 °C for 2 h under UHV. This process ensures a pristine surface free of water and organic molecules. Before the growth was started, the substrates were additionally degassed at 870 °C for 60 min in the growth chamber. This process leads to formation of pinholes in the native oxide.[15] The substrate temperature was then lowered to 634 °C, as measured by a pyrometer. We proceeded with a 40 min Ga predeposition step, with a flux corresponding to a GaAs growth rate of 1 Å/s. For NW growth, the As_4 source was opened for 16 min at a beam equivalent pressure of 2×10^{-6} Torr.

Received: January 26, 2021
Revised: March 30, 2021
Published: April 5, 2021

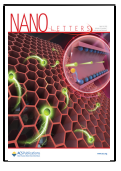

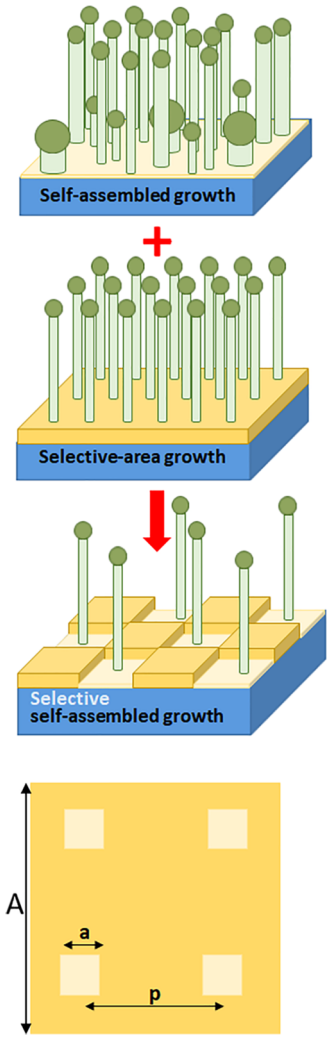

Figure 1. Illustration of the localized self-assembled growth principle. This method aims at obtaining ordered NW arrays with a narrow morphological distribution without nanoscale surface patterning. The growth area size (a) and the pitch (p) determine the arrangement of the NW array. The cross-sectional schematic shows the thermal oxide positioning and the self-catalyzed growth of NWs through the pinholes.

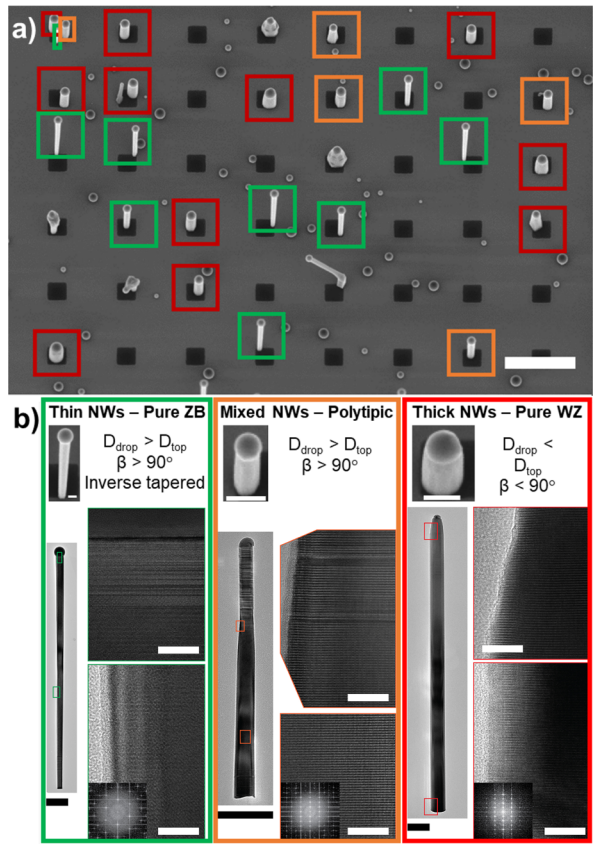

Figure 2. (a) SEM images (with a 20° tilt) of GaAs NWs grown by the localized self-assembled method. The scale bar represents 1 μm. Three distinct shapes of GaAs NWs can be identified: (i) thin and long NWs with the pronounced inverse tapering and the largest contact angles (green frames), (ii) mixed NWs (with a slight tapering) having intermediate contact angles and shorter lengths (orange frames), and (iii) thick NWs with the shortest lengths, whose droplets are smaller than the top facet and the contact angles are smaller than 90° (red frames). (b) TEM and HR TEM images with the corresponding FFTs of thin, mixed, and thick NWs, revealing the ZB phase of the thin NW and the WZ phase of the thick and mixed NWs. The scale bars represent 200 nm for the entire NWs and 10 nm in the HR images.

Figure 2a shows a typical scanning electron micrograph (SEM) of the resulting GaAs NWs grown on patterned silicon substrates with a = 250 nm and p = 1 μm. We observe the formation of NWs in the patterned areas. Not all openings are filled. Most of them contain one NW, and few of them exhibit a second NW. Three distinct NW morphologies can be identified in relation with the contact angle of the Ga catalyst droplet.[16] The first kind of NW exhibits an aspect ratio (AR, axial length over average diameter) between 10 and 20 and is characterized by inverse tapering and large contact angles of the droplet (β > 130°). We will refer to these NWs as "thin NWs" in the following (green frames in Figure 2a). Other nanowires exhibit a thick and short morphology (AR = 1−3) with no tapering and β < 90° ("thick NWs", red frames in Figure 2a). Finally, some NWs show intermediate (mixed) features: that is, a low aspect ratio and intermediate contact angles β larger than 100° ("mixed NWs", orange frames in Figure 2 (a)).

The crystal phase of GaAs NWs exhibiting different morphologies was investigated by high-resolution transmission electron microscopy (TEM). Figure 2b shows different crystal phases that are observed depending on the morphology. A representative thin NW is shown on the left of the micrograph. The contrast along the NW is homogeneous, indicating a single-crystal phase of the entire NW except for the very tip. High-resolution TEM (HR TEM) images obtained from the {110} zone axis and the corresponding fast Fourier transforms (FFTs) are shown in the insets. They indicate a pure zincblende (ZB) phase along the NW and a 10 nm thick polytypic area at the tip, corresponding to the end of growth. A TEM image of a typical thick NW, imaged along the {11−20} zone axis, is shown on the right of Figure 2b. The homogeneous contrast indicates again a single-crystal phase along the most of the NW length. HR TEM and the corresponding FFT reveal the wurtzite (WZ) phase. The NW tip exhibits a polytypic structure. A HR TEM image of a mixed NW is shown in the middle of Figure 2b. Around two-thirds of mixed NWs exhibits the WZ phase, and the rest are

https://doi.org/10.1021/acs.nanolett.1c00349
Nano Lett. 2021, 21, 3139−3145

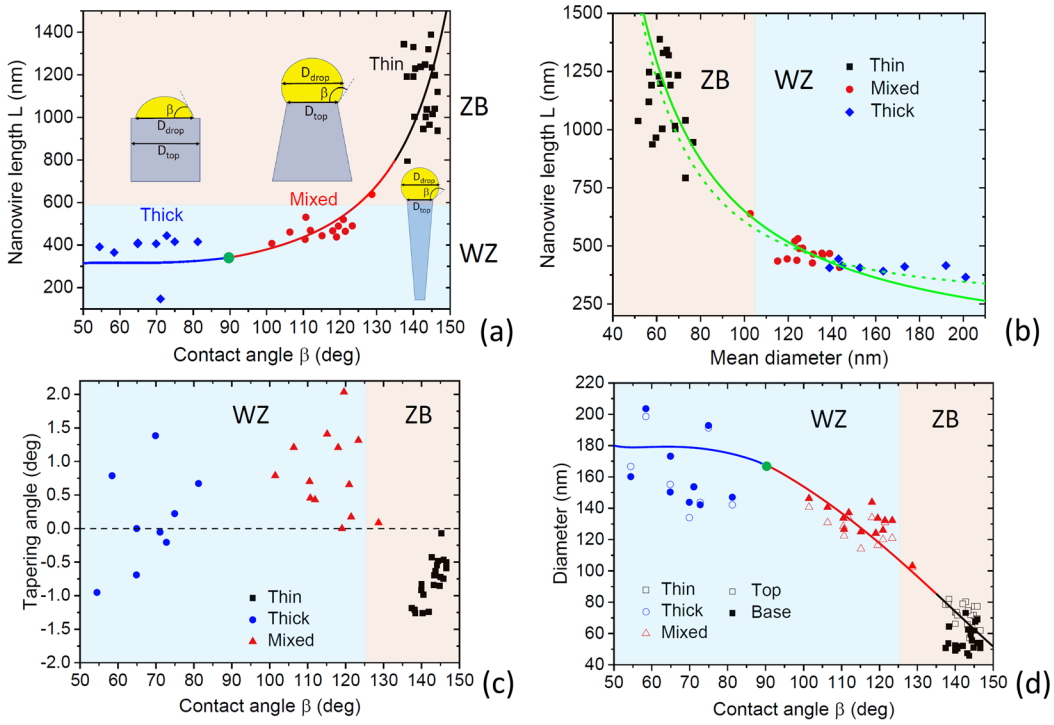

Figure 3. (a) NW length versus the contact angle of Ga droplets. The insets show the NW shapes and the measured parameters (D_{drop}, D_{top}, β) for the three types of NWs (thin, mixed, and thick) The NW length increases quire abruptly with β. (b) NW length versus the mean NW diameter (measured at half of the length for tapered NWs), revealing a sharply decreasing length−diameter correlation. (c) Tapering angles for the three populations of NWs, showing that thick NWs are untapered, mixed NWs are tapered, and thin NWs are inverse tapered. (d) NW top and base diameters versus the contact angle, demonstrating that thinner NWs have larger contact angles of their Ga droplets. The domains of the WZ and ZB crystal phases in each graph are separated by the critical contact angle $\beta_c = 125°$ in (c) and (d), which corresponds to the critical length of ∼600 nm in (a) and the critical diameter of ∼105 nm in (b). Green dots in (a) and (d) correspond to $\beta = 90°$, below which the NWs start losing their Ga droplets. The line in (a) is the fit obtained from eqs 1 and 2. The solid line in (b) is the fit obtained from eqs 1 and 6. The dashed line shows the fit obtained from the general model for the Ga collection given by eq 4 with $\Lambda_f = 280$ nm and $\Lambda_s = 65$ nm and is not much better than the simplified model. The line in (d) is the fit obtained from eq 6.

characterized by a more polytypic structure with the majority of the WZ phase with some ZB insertions.

We will now try to understand why thicker and shorter GaAs NWs are WZ, while thinner and longer GaAs NWs are ZB, as shown in Figure 2. We note that the observed trend for the predominant WZ crystal phase of thicker NWs is very unusual and is opposite to that predicted by earlier thermodynamic[17,18] or kinetic[19,20] models of polytypism in III−V NWs. Indeed, a simple interplay of surface and volume contributions into the NW formation energy[18] or a more complex considerations of two-dimensional (2D) nucleation at the triple-phase line[19,20] naturally lead to a certain critical radius separating the domains of predominantly WZ (below the critical radius) and ZB (above the critical radius) crystal phases of the vapor−liquid−solid (VLS) III−V NWs. Recent *in situ*[21] and *ex situ*[22] data show, however, that the main parameter controlling the crystal phase of self-catalyzed GaAs NWs is the droplet contact angle β. In particular, WZ GaAs NWs with vertical side facets and a planar liquid−solid interface under the droplet form in the range of contact angles from 90−100° to 125°. Here, 2D nucleation occurs at the triple-phase line[20] or even at the edges separating the facets[23] and the WZ phase is preferred due to a lower energy of relevant crystal planes. Above the critical contact angle $\beta_c = 125°$, the surface energetics favors the truncation of the growth interface,[21,24] which is why 2D nucleation occurs away from the triple-phase line and GaAs NWs form in the ZB phase. The effective surface energy of the growth interface considered in refs 21 and 24−27 is independent of the NW radius and hence the phase selection rules are expected to be similar for differently sized NWs provided that the VLS growth is mononuclear.[19,20]

A statistical analysis of the image shown in Figure 1 reveals three different NW shapes, which are presented in Figure 2. Statistical data are shown in Figure 3. Thin NWs are inverse tapered and have the largest lengths (from 800 to 1400 nm) and the largest contact angles of Ga droplets, which are systematically greater than 130°. Mixed NWs are slightly tapered and shorter in length (between ∼400 and ∼600 nm), and the contact angles of their Ga droplets are typically between 100 and 125°. In both populations, the measured maximum diameter of the droplet (D_{drop}) is larger than the diameter of the top NW facet (D_{top}) and the droplets entirely cover the top facet. Since $\sin \beta = D_{top}/D_{drop}$, β is larger than 90°. Thick NWs are the shortest, with typical lengths being slightly above 400 nm, and are restricted by vertical sidewalls. Their Ga droplets are smaller than the top facet ($D_{drop} < D_{top}$), and the contact angles are smaller than 90°. This should be due to an insufficient supply of Ga to the droplet, where the contact angle decreases below the equilibrium Young angle and the droplet unpins from the NW periphery.[22] Most importantly, short (mixed and thick) NWs are WZ, while thin and long NWs are ZB.

According to refs 28−30, the axial growth rate of self-catalyzed GaAs NWs is proportional to the atomic input of As:

https://doi.org/10.1021/acs.nanolett.1c00349
Nano Lett. 2021, 21, 3139−3145

$$\frac{dL}{dt} = \chi(\beta) v_S \tag{1}$$

Here, v_S is the atomic flux of As which includes the re-emitted species[30] and $\chi(\beta)$ is the geometrical function of MBE growth given by[31]

$$\chi(\beta) = \frac{1}{\sin^2\beta} \quad \beta > \alpha + \pi/2$$

$$\chi(\beta) = \frac{1}{\pi \sin^2\beta}\left[\frac{\pi}{2} - \arcsin\left(\frac{\cos\beta}{\sin\alpha}\right) - \cos\beta + \cos\alpha \sin^2\beta \arcsin\left(\frac{\sqrt{\sin^2\beta - \cos^2\alpha}}{\sin\alpha \sin\beta}\right)\right]$$

$$\pi/2 < \beta < \alpha + \pi/2$$

$$\chi(\beta) = \frac{1}{\pi \sin^2\beta}\left[\cos\alpha \sin^2\beta \arcsin(\cot\alpha \cot\beta) - \cos\beta \sqrt{\sin^2\beta - \cos^2\alpha} + \arcsin\left(\frac{\sqrt{\sin^2\beta - \cos^2\alpha}}{\sin\alpha}\right)\right]$$

$$\pi/2 - \alpha < \beta < \pi/2 \tag{2}$$

In our MBE system, the beam angle α equals 45° for both As and Ga species. Clearly, the χ function increases for larger contact angles β, meaning that larger droplets collect more As atoms.

The change of droplet volume V can be determined as

$$\frac{dV}{dt} = \frac{\Omega_L}{\Omega_S}\pi R^2 (F_3 v_3 - \chi v_S) \tag{3}$$

Here, $\Omega_L/\Omega_S = 0.442$ is the ratio of elementary volume of liquid Ga over the volume of the GaAs pair in solid, R is the NW radius, $v_3 = 8.5$ nm/min is the atomic flux of Ga in our experiment, and F_3 collects different kinetic pathways of Ga into the droplet which will be discussed shortly. A nonstationary droplet can change its volume by increasing or decreasing its base radius R or contact angle β.[32] According to the data of ref 21, GaAs NWs are restricted by vertical sidewalls in the range of contact angles from ~90 to 127°, which is the interesting domain in which the WZ NWs form. In this case, the droplet volume equilibrates by changing its contact angle at a constant R according to $d\beta/Ld = (\Omega_L/\Omega_S)[(1 + \cos\beta)^2/R][F_3 v_3/\chi v_S - 1]$. An analysis of this equation shows that the length segment corresponding to the contact angle change is on the order of R under our growth conditions. Therefore, β quickly equilibrates over a short length segment at the beginning of growth and further evolution proceeds at a time-independent β. More details are given in the Supporting Information. Using approximately β = const for all growth times, we can write $L = \chi(\beta) v_S t$. The curve in Figure 3a is obtained from this expression and eq 2 at $v_S t$ = 400 nm and gives an excellent fit to all the data except for the thickest NWs (whose growth kinetics is slightly different because the droplet shrinks less than the top facet).

The morphology and the related crystal phase of our NWs can now be understood as follows. The VLS growth of GaAs NWs is catalyzed by Ga droplets that have different sizes due to their random nucleation in the square pinholes. Smaller droplets produce thinner NWs, and their contact angle is well above the critical value of 125°. These thin NWs grow more quickly due to a more efficient collection of As atoms from the vapor, while their crystal phase is ZB. According to ref 21, ZB GaAs NWs are restricted by outward-tapered side facets when β exceeds 127°, which explains the observed inverse tapering of thin NWs. Such a shape is often seen in the ensembles of self-catalyzed ZB GaAs NWs.[33] Larger droplets yield thicker NWs, and their contact angle is smaller than 125°, which is why mixed and thick NWs are WZ. Tapering of mixed NWs should be due to radial growth occurring after the crystal phase has been decided. However, these considerations do not explain why Ga droplets resting on top of thinner NWs exhibit larger contact angles. To elaborate on this, we use the data shown in Figure 2b. The decreasing length−diameter dependence is typical for group III limited VLS growth of Au-catalyzed III−V NWs driven by surface diffusion of group III adatoms[34−37] but has not been observed for self-catalyzed GaAs NWs to our knowledge. In sharp contrast to Au-catalyzed NWs, group V limited self-catalyzed VLS growth has previously been considered almost insensitive to the NW radius,[28−30] which is why the present results call for an investigation.

We study the unusual radius dependence of the NW growth rate and crystal phase by considering the mass transport of Ga atoms at a constant droplet volume where $dL/dt = \chi v_S = F_3 v_3$ according to eq 3. According to refs 34−37, Ga atoms are collected by (i) direct impingement onto the droplet surface, (ii) diffusion from the NW sidewalls, and (iii) diffusion from the substrate surface, where the interplay between different kinetic pathways depends on the NW length, radius, and Ga collection lengths on the sidewalls and substrate. With neglect of a slight tapering seen in some of our NWs, the Ga-limited axial growth rate is given by[35,36]

$$\frac{dL}{dt} = \left[\chi(\beta) + \frac{2L \sin\alpha}{\pi R} + \left(\frac{2\Lambda_s}{R} + \frac{\Lambda_s^2}{R^2}\right)\cos\alpha\right] v_3 \quad L \le \Lambda_f$$

$$\frac{dL}{dt} = \left[\chi(\beta) + \frac{2\Lambda_f \sin\alpha}{\pi R}\right] v_3 \quad L > \Lambda_f \tag{4}$$

Here, $\chi(\beta)$ is the same geometrical function as in eq 2 and describes the direct impingement of Ga atoms onto the droplet. The second term in eq 4 at $L \le \Lambda_f$ describes the Ga collection from the entire NW length. The third term gives the contribution from Ga adatoms diffusing from the substrate surface, with Λ_s as the characteristic diffusion length determining the width of the feeding ring. At $L > \Lambda_f$, the contribution from the substrate disappears, while the Ga collection length on the NW sidewalls equals the corresponding diffusion length Λ_f.[36] All terms in eq 4 are proportional to the Ga deposition rate v_3. A simpler geometrical approximation was proposed in ref 37

$$\frac{dL}{dt} = \left[\chi(\beta) + \frac{2\lambda \sin\alpha}{\pi R} + \frac{A^2 \cos\alpha}{\pi R^2}\right] v_3 \tag{5}$$

where the second and the third terms in brackets describe Ga adatoms diffusing from the NW sidewalls and the substrate, respectively. Hence, λ is the effective collection length of Ga adatoms on the NW sidewalls, while A^2 is the effective collection area of Ga adatoms on the substrate surface (within the square openings in our case). These parameters are related

https://doi.org/10.1021/acs.nanolett.1c00349
Nano Lett. 2021, 21, 3139−3145

to Λ_s and Λ_f in eq 4. The growth rate given by eq 5 is independent of the NW length, and hence $L = [\chi(\beta)] + 2\lambda \sin \alpha/\pi R + A^2 \cos \alpha/\pi R^2]v_3 t$. As shown in the Supporting Information, eq 5 yields a good approximation to the more general model given by eq 4 when the Ga diffusion length on the NW sidewalls is sufficiently short.

In our experiments, the 2D equivalent growth rate $v_3 \cos \alpha$ = 0.1 nm/s and therefore the 2D equivalent deposition thickness $v_3 \cos \alpha t$ = 96 nm or $v_3 t$ = 136 nm. Comparing this to $v_5 t$ = 400 nm yields the atomic V/III flux ratio v_5/v_3 = 2.94. Equating the As-limited NW length given by eq 1 to the Ga-limited NW length given by eq 5, we obtain the relationship between the NW radius and the contact angle in the form

$$\chi(\beta) = \frac{1}{v_5/v_3 - 1}\left(\frac{2\lambda \sin \alpha}{\pi R} + \frac{A^2 \cos \alpha}{\pi R^2}\right) \quad (6)$$

Using this in eq 1 yields the NW length as a function of its radius, which contains the $1/R$ and $1/R^2$ radius-dependent terms according to eq 6. This radius dependence originates from the material balance of Ga in the steady-state VLS growth at a time-independent droplet volume.

The curves in Figures 3b,d show the best fits to the NW length versus the diameter and the NW diameter versus the contact angle, obtained from eqs 1 and 6 with A = 100 nm and λ = 250 nm. The effective collection area of Ga adatoms on the substrate appears to be smaller than the pinhole area (a = 250 nm). A short collection length on the sidewalls of only 250 nm confirms the validity of the approximate eq 5. As a result, the curve in Figure 3b obtained from a more general eq 4 for Ga diffusion is only slightly different from the approximate curve. With these fits, the critical length and diameter corresponding to the ZB to WZ crystal phase transition equal 600 and 105 nm, respectively. The WZ phase forms in shorter and thicker GaAs NWs.

Thus, we were able to explain the unusual effect of the WZ phase formation in thicker self-catalyzed GaAs NWs by considering the NW growth rate as a function of the droplet contact angle and the NW diameter, which is predetermined by the size of Ga droplets forming in the square pinholes. The surface diffusion of Ga adatoms is slower for thicker NWs, which is why their Ga droplets have smaller contact angles (<125°) and the NW axial growth rate is lower. Thick and short NWs form in the WZ phase. Conversely, surface diffusion of Ga adatoms is largely enhanced for thinner NWs, which increases the droplet contact angle above the critical value of 125° and simultaneously enhances the axial growth rate. Therefore, thin and long NWs adopt the ZB phase. It is remarkable that both ZB and WZ GaAs NWs can be obtained under identical MBE growth conditions within one sample, because the crystal phase is determined simply by the size of Ga droplets. We have identified two trends in self-catalyzed GaAs that have not been noticed before. First, the material balance of Ga yields a decreasing length−radius correlation similarly to the Au-catalyzed VLS growth. Although the self-catalyzed VLS growth is As-limited, a larger amount of Ga arriving into the droplets of thinner NWs increases the contact angle and hence they grow more quickly by collecting more As atoms. The situation is reversed for thicker NWs whose droplets are smaller, which suppresses the growth rate. Second, thicker self-catalyzed GaAs NWs form in the WZ phase, opposite to the common view. This effect originates from the interplay among the Ga surface diffusion, NW radius, and contact angle as discussed above.

In conclusion, we have demonstrated a modification of the selective area epitaxy technique to grow self-catalyzed GaAs NWs on silicon, in which self-assembly of the NWs occurs in the reduced regions on a patterned substrate. The method allows one to obtain the growth selectivity without costly surface preparation and can be extended to other material systems. Ga droplets are formed in the Ga predeposition step by random nucleation within patterned pinholes in the native oxide, leading to a broad size distribution. Further optimization of the process is required to reduce the size inhomogeneity. However, differently sized droplets enable simultaneous growth of the WZ and ZB NWs. Larger droplets produce thicker NWs, which collect fewer Ga atoms by surface diffusion, which is why the contact angles of Ga droplets are small and the crystal phase is WZ. Smaller droplets produce thinner NWs whose droplets inflate due to higher Ga diffusion fluxes. The droplet contact angles in thin NWs are large and hence the crystal phase is ZB. We have demonstrated a pure WZ phase in GaAs NWs up to 200 nm in diameter. Their length can easily be increased by using longer deposition times if required. Overall, the trend of forming the WZ phase in thick GaAs NWs is reported and analyzed for the first time to our knowledge. The possibility of obtaining different crystal phases in one growth run can be used in further studies of polytypism in III−V NWs. The droplet size has been identified as the simple tuning knob for the crystal phase selection, which can be utilized in different protocols for Au-free growth of III−V NWs on silicon substrates.

METHODS

The NWs were grown on p-doped (111) silicon wafers with a resistivity of <0.03 Ω cm (nominal doping concentration of 10^{18} cm^{-3}). The substrates were diced into 20 × 20 mm^2 square chips. The growth area array was patterned through electron-beam lithography on ZEP positive resist (1:1 copolymer of α-chloro methacrylate and methylstyrene), spin-coated on the substrates. The pattern was transferred on the oxide layer by dry etching using CHF_3/SF_6 chemistry. The roughness of the mask was controlled by dipping the substrates 2 s in 7:1 buffered hydrofluoric acid solution (BHF), while a 10 s dip HF solution (1%) was used to remove the native oxide from the bottom of the growth area. A thin native oxide (~1.1 nm) layer was grown in these areas using O_2 plasma in TEPLA GigaBatch for 30 s at 200 W power, with 200 sccm O_2 flow and a pressure of 0.5 bar. The final oxide thickness was monitored with a Sopra GES 5E spectroscopic ellipsometer.

The as-prepared chips were introduced into the ultrahigh vacuum (UHV) environment of an MBE machine (DCA P600) and subsequently annealed at 500 °C for 2 h under UHV to ensure a pristine surface free of water and organic molecules. Before the growth was started, the chips were transferred to the growth chamber, where they were degassed at 870 °C for 60 min to further increase the density of pinholes in the native oxide. Ga was predeposited for 40 min at a substrate temperature of 634 °C, measured by a pyrometer, and with 7 rpm rotation, with a flux corresponding to the GaAs growth rate of 1 Å/s. The As_4 source was opened for 16 min at a beam equivalent pressure (BEP) of 2 × 10^{-6} Torr.

TEM and HRTEM images were obtained by mechanically transferring grown nanowires onto a copper grid with

https://doi.org/10.1021/acs.nanolett.1c00349
Nano Lett. 2021, 21, 3139−3145

amorphous carbon. They were done using a Talos F200S G2 TEM with a double-tilt holder at 100 keV beam voltage.

■ ASSOCIATED CONTENT

Supporting Information

The Supporting Information is available free of charge at https://pubs.acs.org/doi/10.1021/acs.nanolett.1c00349.

Details of the model (PDF)

■ AUTHOR INFORMATION

Corresponding Author

Vladimir G. Dubrovskii − *Faculty of Physics, St. Petersburg State University, 199034 St. Petersburg, Russia;* orcid.org/0000-0003-2088-7158; Email: dubrovskii@mail.ioffe.ru

Authors

Wonjong Kim − *Laboratory of Semiconductor Materials, Institute of Materials, Faculty of Engineering, Ecole Polytechnique Fédérale de Lausanne, 1015 Lausanne, Switzerland*

Valerio Piazza − *Laboratory of Semiconductor Materials, Institute of Materials, Faculty of Engineering, Ecole Polytechnique Fédérale de Lausanne, 1015 Lausanne, Switzerland*

Lucas Güniat − *Laboratory of Semiconductor Materials, Institute of Materials, Faculty of Engineering, Ecole Polytechnique Fédérale de Lausanne, 1015 Lausanne, Switzerland;* orcid.org/0000-0001-7883-4433

Anna Fontcuberta i Morral − *Laboratory of Semiconductor Materials, Institute of Materials, Faculty of Engineering, Ecole Polytechnique Fédérale de Lausanne, 1015 Lausanne, Switzerland; Institute of Physics, Faculty of Basic Sciences, Ecole Polytechnique Fédérale de Lausanne, 1015 Lausanne, Switzerland;* orcid.org/0000-0002-5070-2196

Complete contact information is available at: https://pubs.acs.org/10.1021/acs.nanolett.1c00349

Author Contributions

W.K., V.P., L.G., and A.F.M. designed and conducted the growth experiments and characterization. A.F.M. supervised the project. V.G.D. did the modeling part. All authors contributed to writing the manuscript.

Funding

W.K., L.G., V.P., and A.F.M. acknowledge funding through the H2020 ITN project INDEED, the SNSF NCCR QSIT, and SNSF project No. 69908 as well as Piaget. V.G.D. gratefully acknowledges financial support from the Russian Science Foundation under Grant No. 19-72-30004.

Notes

The authors declare no competing financial interest.

■ REFERENCES

(1) Cirlin, G. E.; et al. Self-catalyzed, Pure Zincblende GaAs Nanowires Grown on Si(111) by molecular beam epitaxy. *Phys. Rev. B: Condens. Matter Mater. Phys.* **2010**, *82*, 035302.

(2) Glas, F.; Harmand, J.-C.; Patriarche, G. Nucleation Antibunching in Catalyst-Assisted Nanowire Growth. *Phys. Rev. Lett.* **2010**, *104*, 135501.

(3) Heiss, M.; et al. Self-assembled Quantum Dots in a Nanowire System for Quantum Photonics. *Nat. Mater.* **2013**, *12*, 439−444.

(4) Otnes, G.; et al. Strategies to Obtain Pattern Fidelity in Nanowire Growth From Large-area Surfaces Patterned Using Nanoimprint Lithography. *Nano Res.* **2016**, *9*, 2852−2861.

(5) Vukajlovic-Plestina, J.; et al. Engineering the Size Distributions of Ordered GaAs Nanowires on Silicon. *Nano Lett.* **2017**, *17*, 4101−4108.

(6) Kim, W.; Güniat, L.; Fontcuberta i Morral, A.; Piazza, V. Doping Challenges and Pathways to Industrial Scalability of III−V Nanowire Arrays. *Appl. Phys. Rev.* **2021**, *8*, 011304.

(7) Borgström, M. T.; Immink, G.; Ketelaars, B.; Algra, R.; Bakkers, E. P. A. M. Synergetic Nanowire Growth. *Nat. Nanotechnol.* **2007**, *2*, 541−544.

(8) Dubrovskii, V. G.; et al. Self-Equilibration of the Diameter of Ga-Catalyzed GaAs Nanowires. *Nano Lett.* **2015**, *15*, 5580−5584.

(9) Albert, S.; et al. Selective Area Growth of GaN Nanostructures: A Key to Produce High Quality (1120) a-Plane Pseudo-Substrates. *Appl. Phys. Lett.* **2014**, *105*, 091902.

(10) Friedl, M.; et al. Template-Assisted Scalable Nanowire Networks. *Nano Lett.* **2018**, *18*, 2666−2671.

(11) Güniat, L.; Caroff, P.; Fontcuberta i Morral, A. Vapor Phase Growth of Semiconductor Nanowires: Key Developments and Open Questions. *Chem. Rev.* **2019**, *119*, 8958−8971.

(12) Barrigón, E.; Heurlin, M.; Bi, Z.; Monemar, B.; Samuelson, L. Synthesis and Applications of III−V Nanowires. *Chem. Rev.* **2019**, *119*, 9170−9220.

(13) Friedl, M.; et al. Remote Doping of Scalable Nanowire Branches. *Nano Lett.* **2020**, *20*, 3577−3584.

(14) Krogstrup, P.; et al. Single Nanowire Solar Cells Beyond Shockley-Queisser Limit. *Nat. Photonics* **2013**, *7*, 306−310.

(15) Matteini, F.; et al. Tailoring the Diameter and Density of Self-catalyzed GaAs Nanowires on Silicon. *Nanotechnology* **2015**, *26*, 105603.

(16) Ghisalberti, L.; et al. Questioning Liquid Droplet Stability on Nanowire Tips: From Theory to Experiment. *Nanotechnology* **2019**, *30*, 285604.

(17) Akiyama, T.; Nakamura, K.; Ito, T. Structural Stability and Electronic Structures of InP Nanowires: Role of Surface Dangling Bonds on Nanowire Facets. *Phys. Rev. B: Condens. Matter Mater. Phys.* **2006**, *73*, 235308.

(18) Dubrovskii, V. G.; Sibirev, N. V. Growth Thermodynamics of Nanowires and its Application to Polytypism of Zinc Blende III-V Nanowires. *Phys. Rev. B: Condens. Matter Mater. Phys.* **2008**, *77*, 035414.

(19) Dubrovskii, V. G.; Sibirev, N. V.; Harmand, J. C.; Glas, F. Growth Kinetics and Crystal Structure of Semiconductor Nanowires. *Phys. Rev. B: Condens. Matter Mater. Phys.* **2008**, *78*, 235301.

(20) Glas, F.; Harmand, J.-C.; Patriarche, G. Why Does Wurtzite Form in Nanowires of III-V Zinc Blende Semiconductors? *Phys. Rev. Lett.* **2007**, *99*, 146101.

(21) Panciera, F.; et al. Phase Selection in Self-catalyzed GaAs Nanowires. *Nano Lett.* **2020**, *20*, 1669−1675.

(22) Kim, W.; et al. Bistability of Contact Angle and Its Role in Achieving Quantum-Thin Self-Assisted GaAs nanowires. *Nano Lett.* **2018**, *18*, 49−57.

(23) Harmand, J.-C.; et al. Atomic Step Flow on a Nanofacet. *Phys. Rev. Lett.* **2018**, *121*, 166101.

(24) Jacobsson, D.; et al. Interface Dynamics and Crystal Phase Switching in GaAs Nanowires. *Nature* **2016**, *531*, 317−322.

(25) Dubrovskii, V. G. Development of Growth Theory for Vapor−Liquid−Solid Nanowires: Contact Angle, Truncated Facets, and Crystal Phase. *Cryst. Growth Des.* **2017**, *17*, 2544−2548.

(26) Dubrovskii, V. G.; Sibirev, N. V.; Halder, N. N.; Ritter, D. Classification of the Morphologies and Related Crystal Phases of III−V Nanowires Based on the Surface Energy Analysis. *J. Phys. Chem. C* **2019**, *123*, 18693−18701.

(27) Wen, C.-Y.; et al. Periodically Changing Morphology of the Growth Interface in Si, Ge, and GaP Nanowires. *Phys. Rev. Lett.* **2011**, *107*, 025503.

(28) Colombo, C.; Spirkoska, D.; Frimmer, M.; Abstreiter, G.; Fontcuberta i Morral, A. Ga-Assisted Catalyst-Free Growth Mechanism of GaAs Nanowires by Molecular Beam Epitaxy. *Phys. Rev. B: Condens. Matter Mater. Phys.* **2008**, *77*, 155326.
(29) Dubrovskii, V. G.; Group, V. Sensitive Vapor−Liquid−Solid Growth of Au-Catalyzed and Self-Catalyzed III−V Nanowires. *J. Cryst. Growth* **2016**, *440*, 62−68.
(30) Glas, F.; Ramdani, M. R.; Patriarche, G.; Harmand, J. C. Predictive Modeling of Self-Catalyzed III-V Nanowire Growth. *Phys. Rev. B: Condens. Matter Mater. Phys.* **2013**, *88*, 195304.
(31) Glas, F. Vapor Fluxes on the Apical Droplet During Nanowire Growth by Molecular Beam Epitaxy. *Phys. Status Solidi B* **2010**, *247*, 254−258.
(32) Tersoff, J. Stable self-catalyzed growth of III−V nanowires. *Nano Lett.* **2015**, *15*, 6609−6613.
(33) Dubrovskii, V. G.; et al. New Mode of Vapor−Liquid−Solid Nanowire Growth. *Nano Lett.* **2011**, *11*, 1247−1253.
(34) Dubrovskii, V. G.; et al. Diffusion-Controlled Growth of Semiconductor Nanowires: Vapor Pressure Versus High Vacuum Deposition. *Surf. Sci.* **2007**, *601*, 4395−4401.
(35) Plante, M. C.; LaPierre, R. R. Analytical Description of the Metal-assisted Growth of III−V Nanowires: Axial and Radial Growths. *J. Appl. Phys.* **2009**, *105*, 114304.
(36) Dubrovskii, V. G.; Berdnikov, Y.; Schmidtbauer, J.; Borg, M.; Storm, K.; Deppert, K.; Johansson, J. Length distributions of nanowires growing by surface diffusion. *Cryst. Growth Des.* **2016**, *16*, 2167−2172.
(37) Borg, M.; Johansson, J.; Storm, K.; Deppert, K. Geometric Model for Metalorganic Vapour Phase Epitaxy of Dense Nanowire Arrays. *J. Cryst. Growth* **2013**, *366*, 15−19.

https://doi.org/10.1021/acs.nanolett.1c00349
Nano Lett. 2021, 21, 3139−3145